FULL PAPER

Dalton
www.rsc.org/dalton

Synthesis and molecular structures of nitrosoarene metalloporphyrin complexes of ruthenium

Jonghyuk Lee,[a] Brendan Twamley[b] and George B. Richter-Addo*[a]

[a] *Department of Chemistry and Biochemistry, University of Oklahoma, 620 Parrington Oval, Norman, Oklahoma, USA 73019. E-mail: grichteraddo@ou.edu*

[b] *X-ray Structural Laboratory, University Research Office, 109 Morrill Hall, University of Idaho, Moscow, Idaho, USA 83844-3010.*

Received 1st August 2003, Accepted 20th November 2003
First published as an Advance Article on the web 9th December 2003

Several new ruthenium porphyrins containing nitrosoarene ligands have been synthesized and characterized by IR and ^{1}H NMR spectroscopy, and by single-crystal X-ray crystallography. Bis-nitrosoarene complexes of the form (por)Ru(ArNO)$_2$ (Ar = aryl group; por = TPP, TTP; TPP = tetraphenylporphyrinato dianion, TTP = tetratolylporphyrinato dianion) were prepared in good yields from the reaction of the nitrosoarenes with (por)Ru(CO). The IR spectra of the complexes (as KBr pellets) display new bands in the 1346–1350 cm^{-1} region due to ν_{NO}. Reactions of the (por)Ru(ArNO)$_2$ complexes with excess pyridine and 1-methylimidazole produce the mono-nitrosoarene complexes (por)Ru(ArNO)(py) and (por)Ru(ArNO)(1-MeIm), respectively. The IR spectra of these mono-nitrosoarene complexes reveal a lowering of ν_{NO} by 14–44 cm^{-1}, a feature consistent with the replacement of one of the π-acid ArNO ligands with the more basic pyridine and 1-MeIm ligands. The solid-state molecular structures of two members of each of the three classes of compounds, namely (por)Ru(ArNO)$_2$, (por)Ru(ArNO)(py) and (por)Ru(ArNO)(1-MeIm) were determined by single-crystal X-ray diffraction, and reveal the *N*-binding mode of the ArNO ligands.

Introduction

Nitrosoalkanes and nitrosoarenes belong to the general class of *C*-nitroso compounds, and they have extensive coordination chemistry.[1] The ability of nitrosoarenes (ArNO; Ar = aryl group) to bind to metal centers has consequences in biological chemistry. Nitrosoarenes are known to bind to the heme biomolecules such as hemoglobin (Hb) and myoglobin (Mb) which contain histidine-liganded hemes.[1] The binding of *C*-nitroso compounds to cytochrome P450 is also thought to inhibit enzyme activity (reviewed in reference 1). Although no crystal structure of a nitrosoarene adduct of Hb or Mb has been reported, the crystal structure of the nitrosobenzene adduct of the related monomeric leghemoglobin from *Lupinus luteus* is known and reveals an *N*-binding of the PhNO ligand to the iron center of the heme prosthetic group.[2] We recently reported the crystal structure of a nitroso*alkane* adduct of ferrous horse heart myoglobin, namely that of Mb(EtNO).[3] The nitrosoethane ligand was found to bind to the iron center also through the nitroso N-atom. Only a small number of crystal structures of nitrosoarene[4,5] and nitrosoalkane[6,7] complexes of iron porphyrins are known. The study of nitrosoarene ligation to heme centers in biomolecules is particularly important, since such heme–nitrosoarene adducts are products in various metabolic processes involving organonitrogen molecules. For example, the Hb(PhNO) complex is a known metabolic product that results from nitrobenzene poisoning.[8,9]

James and co-workers[10] reported the first synthesis of ruthenium porphyrins containing *C*-nitroso ligands. They prepared the (OEP)Ru(PhNO)$_2$ complex and showed that it converted to the (OEP)Ru(PhNO)(L) (OEP = octaethylporphyrinato dianion; L = CO, PPh$_3$, py) derivatives in solution in the presence of the exogenous ligands. We extended this work to the preparation of (OEP)Ru(N(O)C$_6$H$_4$NMe$_2$-*p*)$_2$ and determined its structure by X-ray crystallography.[11] Elegant work by Che and co-workers[12] resulted in the preparation of the (por)Ru(PhNO)-containing products (por)Ru(PhNO)$_2$, (por)Ru(PhNO)(PhNH$_2$) and (por)Ru(PhNO)(PhNHOH) (por = porphyrinato dianion) from the reactions of dioxoruthenium porphyrins with phenylhydroxylamine. We recently reported a comparative structural analysis of the (TPP)Ru(PhNO)$_2$[12] and (TPP)Ru(PhNO)(1-MeIm) compounds.[13] We were particularly interested in the possible variation in nitrosoarene coordination modes as a function of the substitution in the phenyl ring of the nitrosoarene ligands. For example, it is known that the structures of some *para*-substituted nitrosoarenes have significant dipolar character which places a significant negative charge on the nitroso O-atom; two examples of these nitrosoarenes are shown in Fig. 1. Indeed, we showed that *para*-amino substituted nitrosoarene ligands are capable of *O*-binding to iron[4] and manganese[14] centers in metalloporphyrins.

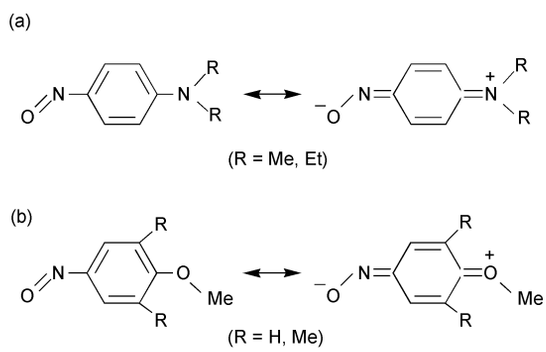

Fig. 1 Two examples of the *C*-nitroso compounds for which dipolar resonance forms are possible: (a) *p*-aminosubstituted nitrosobenzenes and (b) nitrosoanisoles.

In this article, we report the synthesis and spectroscopic characterization of a new series of ruthenium porphyrins of the form (por)Ru(ArNO)$_2$, (por)Ru(PhNO)(py) and (por)Ru(ArNO)(1-MeIm).[15] The spectroscopic data and X-ray crystallographic data provide valuable information on the π-donor and -acceptor properties of the axial ligands, and we demonstrate that significant differences exist in these three classes of compounds.

Experimental

All reactions were performed under an atmosphere of prepurified nitrogen using standard Schlenk glassware and/or in an

DOI: 10.1039/b315051h

Innovative Technology Labmaster 100 Dry Box. Solutions for spectral studies were also prepared under a nitrogen atmosphere. Solvents were distilled from appropriate drying agents under nitrogen just prior to use: CH_2Cl_2 (CaH_2), hexane (CaH_2), toluene (Na).

Chemicals

(TPP)Ru(CO) and (TTP)Ru(CO) were prepared by published procedures (TPP = *meso*-tetraphenylporphyrinato dianion, TTP = *meso*-tetratolylporphyrinato dianion).[16] PhNO (97%), *o*-tolNO (97%), anhydrous pyridine (99.8%) and 1-methylimidazole (1-MeIm, 99+%) were purchased from Aldrich Chemical Company and used as received. 4-Nitrosoanisole (*p*-ONC_6H_4OMe) and 2,6-dimethyl-4-nitrosoanisole (*p*-$ONC_6H_2Me_2OMe$) were prepared by literature methods.[17] $^{15}NOBF_4$ was synthesized by a published procedure[18] using $Na^{15}NO_2$ (99% isotopic purity, Isotec). Chloroform-*d* (99.8%) was obtained from Cambridge Isotope Laboratories.

Instrumentation

Infrared spectra were recorded on a Bio-Rad FT-155 FTIR spectrometer. Proton NMR spectra were obtained on Varian 400 MHz or Varian Mercury VX 300 MHz spectrometers and the signals referenced to the residual signal of $CHCl_3$ at δ 7.24 ppm. All coupling constants are in Hz. FAB mass spectra were obtained on a VG-ZAB-E mass spectrometer. UV-vis spectra were recorded on a Hewlett-Packard model 8453 diode array instrument. Wavelengths are reported with ε values or as percentage intensities for the samples whose yields were too small for accurate concentration measurements. Elemental analyses were performed by Atlantic Microlab, Norcross, Georgia.

Synthesis of *p*-$O^{15}NC_6H_4OMe$

This ^{15}N-labeled 4-nitrosoanisole was synthesized by the direct nitrosation of anisole with $^{15}NOBF_4$ in acetonitrile using the same procedure employed for the preparation of unlabeled *p*-$O^{14}NC_6H_4OMe$.[17] The ^1H NMR spectrum of *p*-$O^{15}NC_6H_4OMe$ was identical to that of *p*-$O^{14}NC_6H_4OMe$. Three bands in the IR spectrum at 1450, 1414 and 762 cm^{-1} of solid *p*-$O^{14}NC_6H_4OMe$[17] showed isotope shifts upon ^{15}N substitution, by −6, −8 and −7 cm^{-1}, respectively.

Preparation of (por)Ru(ArNO)$_2$ compounds (por = TPP, TTP; ArNO = *o*-tolNO, N(O)C_6H_4OMe-*p*, N(O)$C_6H_2Me_2OMe$-*p*)

These compounds were prepared from the reaction of (por)Ru(CO) with an excess of the corresponding nitrosoarene compounds. The following reaction is representative:

(TPP)Ru(CO) (0.100 g, 0.135 mmol) and excess *o*-tolNO (0.050 g, 0.400 mmol) were dissolved in CH_2Cl_2 (30 mL). The reaction mixture was stirred at room temperature for 30 min, during which time it turned from red to brown. The solvent was removed *in vacuo*. The residue was redissolved in CH_2Cl_2 (15 mL), and filtered through a neutral alumina column (2 × 20 cm) in air with CH_2Cl_2 as eluent. The brown band was collected and dried *in vacuo*. The residue was dissolved in a CH_2Cl_2 (15 mL) solution. Slow evaporation of the solvent in air gave crystalline (TPP)Ru(*o*-tolNO)$_2$·0.3CH_2Cl_2 (0.083 g, 0.084 mmol, 63% isolated yield). Anal. Calc. for $C_{58}H_{42}N_6O_2Ru_1$·0.3CH_2Cl_2: C, 71.34; H, 4.37; N, 8.56; Cl, 2.17. Found: C, 71.24; H, 4.46; N, 8.60; Cl, 2.06%. IR (KBr, cm^{-1}): ν_{NO} 1348 s (overlapping with a porphyrin band); also 3054 vw, 3022 vw, 2925 vw, 1596 m, 1574 vw, 1528 w, 1480 w, 1440 w, 1305 m, 1278 w, 1206 w, 1175 w, 1156 w, 1108 vw, 1071 m, 1010 vs, 879 m, 860 m, 834 vw, 794 m, 754 s, 738 w, 714 m, 702 s, 664 w, 620 vw, 527 w. ^1H NMR ($CDCl_3$): δ 8.56 (s, 8H, pyrrole-H of TPP), 8.05 (m, 8H, *o*-H of TPP), 7.70 (m, 12H, *m*,*p*-H of TPP), 6.29 (br, 2H, *p*-H of *o*-tolNO), 5.77 (br, 4H, *m*-H of *o*-tolNO), 5.28 (s, CH_2Cl_2), 1.53 (br, 2H, *o*-H of *o*-tolNO), −1.23 (br, 6H, CH_3 of *o*-tolNO). Low-resolution mass spectrum (FAB): *m*/*z* 835 [(TPP)Ru(*o*-tolNO)]$^+$ (45%), 714 [(TPP)Ru]$^+$ (100%).

The other (por)Ru(ArNO)$_2$ compounds were generated similarly, except for the two nitrosoanisole complexes (TTP)Ru(N(O)C_6H_4OMe-*p*)$_2$ and (TTP)Ru(N(O)$C_6H_2Me_2OMe$-*p*)$_2$ which were synthesized in refluxing toluene (30 min reaction time).

(TTP)Ru(*o*-tolNO)$_2$

71% Isolated yield. IR (KBr, cm^{-1}): ν_{NO} 1350 s (overlapping with a porphyrin band); also 3022 vw, 2956 vw, 2921 vw, 1529 w, 1512 vw, 1480 vw, 1455 vw, 1306 m, 1278 vw, 1263 vw, 1212 w, 1181 m, 1115 w, 1107 w, 1071 m, 1011 vs, 880 m, 859 m, 798 s, 752 m, 719 m, 661 vw, 642 w, 525 m. ^1H NMR ($CDCl_3$): δ 8.57 (s, 8H, pyrrole-H of TTP), 7.93 (d, J = 8, 8H, *o*-H of TTP), 7.49 (d, J = 8, 8H, *m*-H of TTP), 6.25 (br, 2H, *p*-H of *o*-tolNO), 5.73 (br, 4H, *m*-H of *o*-tolNO), 2.68 (s, 12H, CH_3 of TTP), 1.53 (br, 2H, *o*-H of *o*-tolNO), −1.26 (br, 6H, CH_3 of *o*-tolNO). Low-resolution mass spectrum (FAB): *m*/*z* 891 [(TTP)Ru(*o*-tolNO)]$^+$ (24%), 770 [(TTP)Ru]$^+$ (100%).

(TTP)Ru(N(O)C_6H_4OMe-*p*)$_2$

49% Isolated yield. IR (KBr, cm^{-1}): ν_{NO} 1348 s (overlapping with a porphyrin band); also 3020 vw, 2922 vw, 2836 vw, 1595 s, 1584 s, 1528 w, 1497 m, 1461 w, 1439 w, 1425 w, 1329 m, 1304 m, 1257 vs, 1212 w, 1180 m, 1134 s, 1109 m, 1070 m, 1031 m, 1009 vs, 866 m, 833 m, 797 s, 777 w, 716 m, 671 vw, 645 vw, 613 m, 525 m. ^1H NMR ($CDCl_3$): δ 8.52 (s, 8H, pyrrole-H of TTP), 8.01 (d, J = 8, 8H, *o*-H of TTP), 7.50 (d, J = 8, 8H, *m*-H of TTP), 5.43 (br, 4H, *m*-H of N(O)C_6H_4OMe-*p*), 3.35 (br s, 6H, N(O)C_6H_4OMe-*p*), 2.67 (s, 12H, CH_3 of TTP), 2.56 (br, 4H, *o*-H of N(O)C_6H_4OMe-*p*). Low-resolution mass spectrum (FAB): *m*/*z* 907 [(TTP)Ru(N(O)C_6H_4OMe-*p*)]$^+$ (61%), 770 [(TTP)Ru]$^+$ (100%).

(TTP)Ru(^{15}N(O)C_6H_4OMe-*p*)$_2$

IR (KBr, cm^{-1}): ν_{NO} 1318 s.

(TTP)Ru(N(O)$C_6H_2Me_2OMe$-*p*)$_2$

52% Isolated yield. IR (KBr, cm^{-1}): ν_{NO} 1346 s (overlapping with a porphyrin band); also 3022 vw, 2962 w, 2922 w, 2863 vw, 1587 m, 1549 vw, 1528 w, 1474 m, 1447 w, 1413 w, 1304 m, 1263 m, 1222 m, 1180 m, 1105 s, 1070 m, 1009 vs, 967 w, 873 vw, 798 vs, 753 vw, 715 m, 694 w, 526 m. ^1H NMR ($CDCl_3$): δ 8.56 (s, 8H, pyrrole-H of TTP), 7.99 (d, J = 8, 8H, *o*-H of TTP), 7.50 (d, J = 8, 8H, *m*-H of TTP), 3.21 (br s, 6H, N(O)$C_6H_2Me_2OMe$-*p*), 2.67 (s, 12H, CH_3 of TTP), 2.09 (br s, 4H, *o*-H of N(O)$C_6H_2Me_2OMe$-*p*), 1.45 (br s, 12H, N(O)$C_6H_2Me_2OMe$-*p*). Low-resolution mass spectrum (FAB): *m*/*z* 935 [(TTP)Ru(N(O)$C_6H_2Me_2OMe$-*p*)]$^+$ (31%), 770 [(TTP)Ru]$^+$ (100%).

Preparation of (por)Ru(PhNO)(py) compounds (por = TPP, TTP)

These compounds were prepared from the reaction of the corresponding (por)Ru(PhNO)$_2$ with excess pyridine. The following reaction is representative:

To a CH_2Cl_2 solution (10 mL) of (TPP)Ru(PhNO)$_2$[13] (0.020 g, 0.022 mmol) was added ~2 equiv. of pyridine. This mixture was stirred at room temperature for 30 min, during which time it turned from brown to red–purple. The solvent was removed *in vacuo*. A ^1H NMR spectrum of the residue in $CDCl_3$ showed the quantitative formation of (TPP)Ru(PhNO)(py), together with the presence of some unreacted pyridine. Spectroscopically pure (TPP)Ru(PhNO)(py) was obtained in 71% yield by recrystallization of the residue from a CH_2Cl_2–hexane solution (1 : 3) at −20 °C. IR (KBr, cm^{-1}): ν_{NO} 1328 s; also 3075 vw,

3052 w, 3023 w, 1598 m, 1529 w, 1485 w, 1442 m, 1346 m sh, 1308 m sh, 1217 w, 1177 w, 1155 w, 1071 m, 1008 vs, 888 vw, 833 vw, 793 m, 753 s, 714 m, 700 s, 664 w, 527 w. ^{1}H NMR ($CDCl_3$): δ 8.42 (s, 8H, pyrrole-H of TPP), 8.05 (m, 8H, *o*-H of TPP), 7.65 (m, 12H, *m*,*p*-H of TPP), 6.40 (tt, J = 7.2/0.8, 1H, *p*-H of PhNO), 6.09 (tt, J = 7.6/1.6, 1H, *p*-H of pyridine), 5.96 (m, 2H, *m*-H of PhNO), 5.24 (m, 2H, *m*-H of pyridine), 2.55 (m, 2H, *o*-H of PhNO), 1.76 (m, 2H, *o*-H of pyridine). Low-resolution mass spectrum (FAB): *m*/*z* 900 $[(TPP)Ru(PhNO)(py)]^+$ (7%), 851 $[(TPP)Ru(NO)(PhNO)]^+$ (24%), 821 $[(TPP)Ru(PhNO)]^+$ (40%), 793 $[(TPP)Ru(py)]^+$ (9%), 714 $[(TPP)Ru]^+$ (100%). UV-vis spectrum (λ/nm (ε/mM^{-1} cm^{-1})), 3.30 × 10^{-6} M in CH_2Cl_2): 308 (34), 411 (230), 533 (18).

(TTP)Ru(PhNO)(py)

67% Isolated yield. IR (KBr, cm^{-1}): ν_{NO} 1332 s; also 3077 vw, 3023 vw, 2955 vw, 2920 vw, 1602 w, 1528 m, 1510 w, 1487 w, 1445 m, 1400 vw, 1347 m, 1306 m, 1262 w, 1212 w, 1181 m, 1153 w, 1108 m, 1069 m, 1037 vw, 1007 vs, 886 w, 847 vw, 800 s, 794 s, 764 w, 754 w, 715 m, 691 m, 665 vw, 644 vw, 523 m. ^{1}H NMR ($CDCl_3$): δ 8.42 (s, 8H, pyrrole-H of TTP), 7.94 (dd, J = 7.6/1.6, 4H, *o*-H of TTP), 7.90 (dd, J = 7.6/1.6, 4H, *o*′-H of TTP), 7.48 (br d, J = 7.6, 4H, *m*-H of TTP), 7.43 (br d, J = 7.6, 4H, *m*′-H of TTP), 6.36 (tt, J = 7.2/0.8, 1H, *p*-H of PhNO), 6.07 (tt, J = 7.6/1.6, 1H, *p*-H of pyridine), 5.93 (m, 2H, *m*-H of PhNO), 5.22 (m, 2H, *m*-H of pyridine), 2.65 (s, 12H, CH_3 of TTP), 2.52 (m, 2H, *o*-H of PhNO), 1.74 (m, 2H, *o*-H of pyridine). Low-resolution mass spectrum (FAB): *m*/*z* 907 $[(TTP)Ru(NO)(PhNO)]^+$ (46%), 770 $[(TTP)Ru]^+$ (100%). UV-vis spectrum (λ/nm, CH_2Cl_2): 310 (10), 413 (100), 533 (5%).

Preparation of (por)Ru(ArNO)(1-MeIm) compounds (por = TPP, TTP; ArNO = *o*-tolNO, N(O)C_6H_4OMe-*p*, N(O)$C_6H_2Me_2$OMe-*p*).

These compounds were prepared from the reaction of the corresponding $(por)Ru(ArNO)_2$ with excess 1-MeIm. The following reaction is representative:

To a CH_2Cl_2 solution (20 mL) of $(TPP)Ru(o\text{-tolNO})_2\cdot 0.3CH_2Cl_2$ (0.050 g, 0.051 mmol) was added ~2 equiv. of 1-MeIm. This mixture was stirred at room temperature for 30 min, during which time it turned from brown to red–purple. The solvent was removed *in vacuo*. A ^{1}H NMR spectrum of the residue in $CDCl_3$ showed the quantitative formation of (TPP)Ru(*o*-tolNO)(1-MeIm), together with the presence of some unreacted 1-MeIm. Spectroscopically pure $(TPP)Ru(o\text{-tolNO})(1\text{-MeIm})\cdot 0.7CH_2Cl_2$ was obtained in 72% yield by recrystallization of the residue from a CH_2Cl_2–hexane solution (1 : 3) at −20 °C. Anal. Calc. for $C_{55}H_{41}N_7O_1Ru_1\cdot 0.7CH_2Cl_2$: C, 68.51; H, 4.38; N, 10.04; Cl, 5.08. Found: C, 68.75; H, 4.71; N, 9.76; Cl, 5.00%. IR (KBr, cm^{-1}): ν_{NO} 1321 s, 1310 s; also 3125 vw, 3054 vw, 3022 vw, 2952 vw, 2922 vw, 1596 m, 1576 vw, 1530 m, 1486 w, 1439 m, 1347 m, 1334 m, 1277 vw, 1236 w, 1206 w, 1175 w, 1156 vw, 1107 w, 1089 w, 1069 m, 1006 vs, 947 w, 905 w, 834 vw, 818 vw, 793 m, 754 s, 738 m, 713 m, 702 m, 664 w, 648 vw, 616 w, 529 w. ^{1}H NMR ($CDCl_3$): δ 8.37 (s, 8H, pyrrole-H of TPP), 8.01 (m, 8H, *o*-H of TPP), 7.63 (m, 12H, *m*,*p*-H of TPP), 6.26 (ddd (apparent td), J = 7.6/7.6/1.2, 1H, *p*-H of *o*-tolNO), 5.81 (br d, J = 7.6, 1H, *m*-H of *o*-tolNO), 5.74 (br dd (apparent br t), J = 7.6/7.6, 1H, *m*′-H of *o*-tolNO), 5.28 (s, CH_2Cl_2), 4.71 (dd (apparent t), J = 1.2/1.2, 1H of 1-MeIm), 2.16 (s, 3H, CH_3 of 1-MeIm), 2.07 (dd, J = 7.6/1.2, 1H, *o*-H of *o*-tolNO), 1.50 (br, 1H of 1-MeIm), 1.14 (dd (apparent t), J = 1.2/1.2, 1H of 1-MeIm), −0.99 (s, 3H, CH_3 of *o*-tolNO). Low-resolution mass spectrum (FAB): *m*/*z* 917 $[(TPP)Ru(o\text{-tolNO})(1\text{-MeIm})]^+$ (17%), 835 $[(TPP)Ru(o\text{-tolNO})]^+$ (20%), 796 $[(TPP)Ru(1\text{-MeIm})]^+$ (39%), 714 $[(TPP)Ru]^+$ (100%).

The other (por)Ru(ArNO)(1-MeIm) compounds were generated similarly.

(TTP)Ru(*o*-tolNO)(1-MeIm)

58% Isolated yield. IR (KBr, cm^{-1}): ν_{NO} 1311 s; also 3127 vw, 3021 w, 2954 vw, 2921 w, 2867 vw, 1529 m, 1514 w, 1479 w, 1442 w, 1347 m, 1284 w sh, 1237 w, 1211 w, 1181 w, 1108 m, 1090 w, 1072 m, 1008 vs, 947 vw, 906 w, 797 s, 755 w, 718 m, 672 vw, 658 w, 616 vw, 524 m. ^{1}H NMR ($CDCl_3$): δ 8.38 (s, 8H, pyrrole-H of TTP), 7.90 (dd (overlapping with *o*′-H of TTP), 4H, *o*-H of TTP), 7.87 (dd (overlapping with *o*-H of TTP), 4H, *o*′-H of TTP), 7.45 (br d, J = 7.6, 4H, *m*-H of TTP), 7.41 (br d, J = 7.6, 4H, *m*′-H of TTP), 6.23 (br ddd (apparent br td), J = 7.6/7.6/1.2, 1H, *p*-H of *o*-tolNO), 5.78 (br d, J = 7.6, 1H, *m*-H of *o*-tolNO), 5.71 (br dd (apparent br t), J = 7.6/7.6, 1H, *m*′-H of *o*-tolNO), 4.68 (dd (apparent t), J = 1.6/1.6, 1H of 1-MeIm), 2.64 (s, 12H, CH_3 of TTP), 2.14 (s, 3H, CH_3 of 1-MeIm), 2.05 (br dd, J = 7.6/1.2, 1H, *o*-H of *o*-tolNO), 1.47 (br, 1H of 1-MeIm), 1.11 (dd (apparent t), J = 1.6/1.6, 1H of 1-MeIm), −1.01 (s, 3H, CH_3 of *o*-tolNO). Low-resolution mass spectrum (FAB): *m*/*z* 973 $[(TTP)Ru(o\text{-tolNO})(1\text{-MeIm})]^+$ (10%), 891 $[(TTP)Ru(o\text{-tolNO})]^+$ (26%), 852 $[(TTP)Ru(1\text{-MeIm})]^+$ (45%), 770 $[(TTP)Ru]^+$ (100%).

(TTP)Ru(N(O)C_6H_4OMe-*p*)(1-MeIm)

70% Isolated yield. IR (KBr, cm^{-1}): ν_{NO} 1323 s, 1306 s; also 3127 vw, 3021 w, 2921 w, 1599 w, 1563 w, 1528 m, 1510 w, 1497 m, 1460 w, 1441 w, 1348 m, 1246 s, 1212 w, 1182 m, 1156 w, 1108 m, 1093 w, 1072 m, 1034 w, 1008 vs, 947 vw, 903 w, 831 w, 797 s, 717 m, 671 w, 616 w, 524 w. ^{1}H NMR ($CDCl_3$): δ 8.37 (s, 8H, pyrrole-H of TTP), 7.96 (dd, J = 7.6/2.0, 4H, *o*-H of TTP), 7.90 (dd, J = 7.6/2.0, 4H, *o*′-H of TTP), 7.47 (br d, J = 7.6, 4H, *m*-H of TTP), 7.42 (br d, J = 7.6, 4H, *m*′-H of TTP), 5.44 (m, 2H, *m*-H of N(O)C_6H_4OMe-*p*), 4.70 (dd (apparent t), J = 1.2/1.2, 1H of 1-MeIm), 3.40 (s, 3H, N(O)C_6H_4O*Me*-*p*), 2.67 (d (overlapping with CH_3 of TTP), 2H, *o*-H of N(O)C_6H_4OMe-*p*), 2.64 (s, 12H, CH_3 of TTP), 2.15 (s, 3H, CH_3 of 1-MeIm), 1.56 (br, 1H of 1-MeIm), 1.20 (dd (apparent t), J = 1.2/1.2, 1H of 1-MeIm). Low-resolution mass spectrum (FAB): *m*/*z* 989 $[(TTP)Ru(N(O)C_6H_4OMe\text{-}p)(1\text{-MeIm})]^+$ (11%), 907 $[(TTP)Ru(N(O)C_6H_4OMe\text{-}p)]^+$ (19%), 852 $[(TTP)Ru(1\text{-MeIm})]^+$ (35%), 770 $[(TTP)Ru]^+$ (100%).

(TTP)Ru(^{15}N(O)C_6H_4OMe-*p*)(1-MeIm)

IR (KBr, cm^{-1}): ν_{NO} 1296 s, 1275 s.

(TTP)Ru(N(O)$C_6H_2Me_2$OMe-*p*)(1-MeIm)

78% Isolated yield. IR (KBr, cm^{-1}): ν_{NO} 1321 s, 1309 s; also 3124 vw, 3019 vw, 2951 vw, 2920 w, 1530 m, 1469 w, 1453 w, 1347 m, 1286 w, 1214 m, 1181 m, 1127 w, 1109 m, 1091 w, 1072 m, 1007 vs, 947 vw, 885 vw, 848 vw, 799 s, 717 m, 615 vw, 524 m. ^{1}H NMR ($CDCl_3$): δ 8.38 (s, 8H, pyrrole-H of TTP), 7.95 (dd, J = 7.6/2.0, 4H, *o*-H of TTP), 7.90 (dd, J = 7.6/2.0, 4H, *o*′-H of TTP), 7.47 (br d, J = 7.6, 4H, *m*-H of TTP), 7.42 (br d, J = 7.6, 4H, *m*′-H of TTP), 4.71 (dd (apparent t), J = 1.2/1.2, 1H of 1-MeIm), 3.27 (s, 3H, N(O)$C_6H_2Me_2O$*Me*-*p*), 2.65 (s, 12H, CH_3 of TTP), 2.22 (s, 2H, *o*-H of N(O)$C_6H_2Me_2$OMe-*p*), 2.16 (s, 3H, CH_3 of 1-MeIm), 1.59 (br, 1H of 1-MeIm), 1.45 (s, 6H, N(O)C_6H_2*Me*$_2$OMe-*p*), 1.23 (dd (apparent t), J = 1.2/1.2, 1H of 1-MeIm). Low-resolution mass spectrum (FAB): *m*/*z* 1017 $[(TTP)Ru(N(O)C_6H_2Me_2OMe\text{-}p)(1\text{-MeIm})]^+$ (14%), 935 $[(TTP)Ru(N(O)C_6H_2Me_2OMe\text{-}p)]^+$ (17%), 852 $[(TTP)Ru(1\text{-MeIm})]^+$ (37%), 770 $[(TTP)Ru]^+$ (100%).

Solid-state structural determinations

Crystals of representative compounds were grown as follows: $(TTP)Ru(o\text{-tolNO})_2\cdot CH_2Cl_2$ (**1**; CH_2Cl_2–hexane (1 : 2), −20 °C, 3 weeks), $(TTP)Ru(N(O)C_6H_2Me_2OMe\text{-}p)_2$ (**2**; CH_2Cl_2–hexane (1 : 10), −20 °C, 3 days), $(TPP)Ru(PhNO)(py)\cdot CH_2Cl_2$ (**3**; CH_2Cl_2–hexane (1 : 3), −20 °C, 1 week), (TTP)Ru(PhNO)(py)

(**4**; CH_2Cl_2–hexane (1 : 5), −20 °C, 2 weeks), (TPP)Ru(*o*-tolNO)-(1-MeIm)·2.5PhMe (**5**; toluene–hexane (5 : 1), −20 °C, 1 week) and (TTP)Ru(N(O)$C_6H_2Me_2$OMe-*p*)(1-MeIm)·0.5C_6H_{14} (**6**; CH_2Cl_2–hexane (1 : 1), slow evaporation at room temperature).

Structure solution. Data for **1**,**2**,**4**,**5** and **6** were collected at 203(2) K. Data for **3** was collected at 208(2) K. Data were collected using a Bruker/Siemens SMART 1K instrument (Mo-Kα radiation, $\lambda = 0.71073$ Å) equipped with a LT2A low-temperature device. Data were measured using omega scans of 0.3° per frame for 30 s (**1**, **2**, **3**, **5** and **6**) and 50 s (**4**); a half sphere of data totaling 1471 frames was collected for **1**, **3**, **4** and **5**; a full sphere of data with 2132 frames was collected for **2** and **6**. The first 50 frames were recollected at the end of each data collection to monitor for decay. Cell parameters were retrieved using SMART[19] software and refined using SAINTPlus[20] on all observed reflections. Data reduction and correction for Lorentz polarization and decay were performed using the SAINTPlus software. Absorption corrections were applied using SADABS.[21] The structures were solved by direct methods and refined by least squares method on F^2 using the SHELXTL program package.[22] All non-hydrogen porphyrin atoms were refined anisotropically. Solvent molecules presented problems in **1**, **5** and **6**. The CH_2Cl_2 solvent in **1** is disordered with a shared Cl atom. The disorder was refined at 60% for the major fraction. Soft restraints were applied in **5** to keep the toluene solvent molecule geometries similar. The half-occupied toluene was held isotropic. In compound **6**, the hexane solvent molecule was held isotropic and C–C distances were restrained. No decomposition was observed during data collection. Details of the data collection and refinement are given in Table 1. Displacement ellipsoids in Figs. 2–4 are drawn at the 35% probability level.

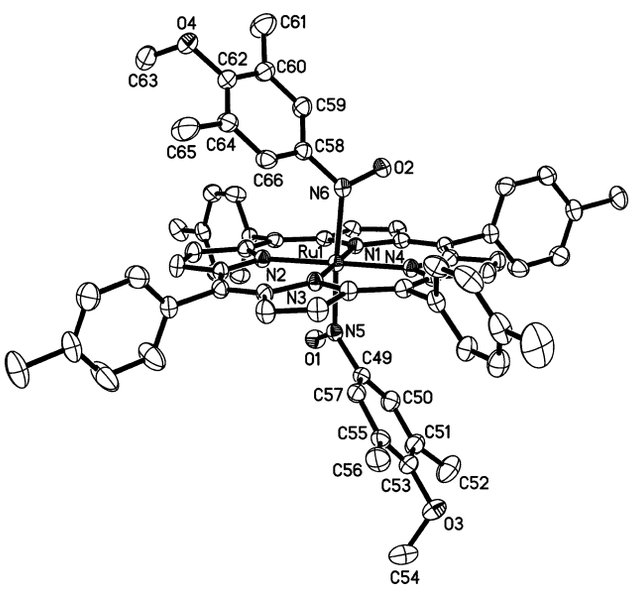

Fig. 2 Molecular structure of (TTP)Ru(N(O)$C_6H_2Me_2$OMe-*p*)$_2$. Hydrogen atoms have been omitted for clarity.

CCDC reference numbers 216560–216565.

See http://www.rsc.org/suppdata/dt/b3/b315051h/ for crystallographic data in CIF or other electronic format.

Results and discussion

Bis-nitrosoarene complexes

The formation of the bis-nitrosoarene complexes from the reaction of (por)Ru(CO) compounds with nitrosoarenes has been reported previously.[10,11,13] Using similar methodology, we have prepared a new series of (por)Ru(ArNO)$_2$ compounds

Table 1 Crystal data and structure refinement

	(TTP)Ru(*o*-tolNO)$_2$·CH_2Cl_2	(TTP)Ru(N(O)-$C_6H_2Me_2$OMe-*p*)$_2$	(TPP)Ru(PhNO)(py)·CH_2Cl_2	(TTP)Ru(PhNO)(py)	(TPP)Ru(*o*-tolNO)-(1-MeIm)·2.5PhMe	(TTP)Ru(N(O)$C_6H_2Me_2$OMe-*p*)-(1-MeIm)·0.5C_6H_{14}
Formula (fw)	$C_{63}H_{52}Cl_2N_6O_2Ru$ (1097.08)	$C_{66}H_{58}N_6O_4Ru$ (1100.25)	$C_{56}H_{40}Cl_2N_6ORu$ (984.91)	$C_{59}H_{46}N_6ORu$ (956.09)	$C_{72.5}H_{61}N_7ORu$ (1147.35)	$C_{64}H_{60}N_7O_2Ru$ (1060.26)
T/K	203(2)	203(2)	208(2)	203(2)	203(2)	203(2)
Crystal system	Triclinic	Triclinic	Monoclinic	Monoclinic	Triclinic	Triclinic
Space group	*P*$\bar{1}$	*P*$\bar{1}$	$P2_1/c$	$P2_1/c$	*P*$\bar{1}$	*P*$\bar{1}$
a/Å	11.5287(14)	11.5715(13)	11.7076(17)	11.5678(17)	11.544(3)	9.657(2)
b/Å	13.0507(16)	13.1249(15)	16.689(2)	15.866(2)	13.908(3)	12.341(3)
c/Å	17.634(2)	19.296(2)	24.156(4)	25.460(4)	20.029(5)	25.125(6)
a/°	93.730(2)	81.409(2)	90	90	103.322(4)	78.598(4)
β/°	91.415(2)	77.879(2)	100.937(2)	96.597(3)	100.795(4)	84.600(4)
γ/°	100.833(2)	74.698(2)	90	90	99.140(4)	78.606(4)
V/Å^3, *Z*	2598.6(6), 2	2749.9(5), 2	4634.0(12), 4	4642.0(12), 4	3004.5(12), 2	2872.7(11), 2
D_c/g cm^{-3}	1.402	1.329	1.412	1.368	1.268	1.226
Crystal size/mm	0.33 × 0.13 × 0.06	0.25 × 0.15 × 0.09	0.20 × 0.16 × 0.16	0.13 × 0.10 × 0.10	0.30 × 0.18 × 0.10	0.34 × 0.16 × 0.15
μ/mm^{-1}	0.457	0.341	0.502	0.388	0.312	0.321
w R (F^2 all data)	0.1163	0.0897	0.1065	0.1119	0.1977	0.2046
Final *R* (obsd. data)	0.0467	0.0374	0.0466	0.0632	0.0674	0.0723

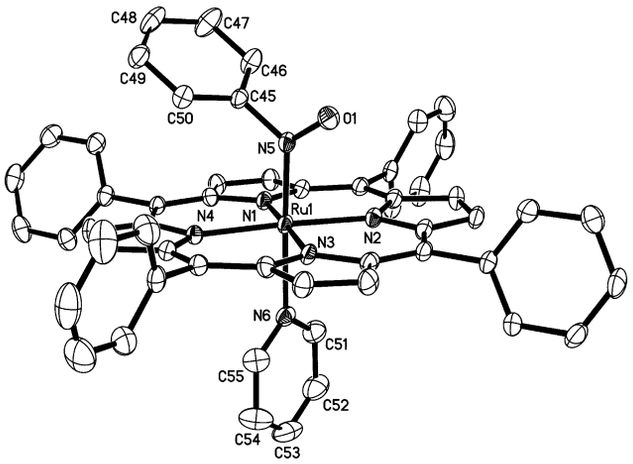

Fig. 3 Molecular structure of (TPP)Ru(PhNO)(py). Hydrogen atoms have been omitted for clarity.

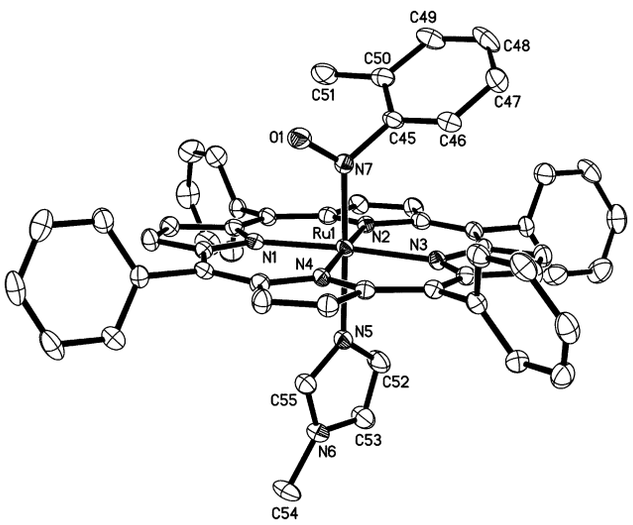

Fig. 4 Molecular structure of (TPP)Ru(*o*-tolNO)(1-MeIm). Hydrogen atoms have been omitted for clarity.

that differ in the nature of porphyrin substitution and the Ar group.

Nitrosoarenes (ArNO = *o*-tolNO, $N(O)C_6H_4OMe$-*p*, $N(O)C_6H_2Me_2OMe$-*p*) react with the (por)Ru(CO) compounds (por = TPP, TTP) in CH_2Cl_2 or refluxing toluene to generate the bis-nitrosoarene complexes (por)$Ru(ArNO)_2$ in 49–71% isolated yields (Scheme 1).

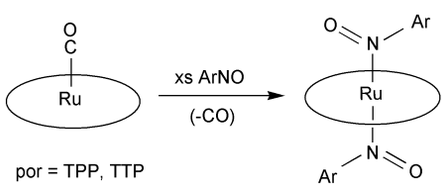

Scheme 1

These brown bis-nitrosoarene complexes are moderately air-stable in solution and can be stored in air in the solid state for several months without noticeable decomposition. They are soluble in CH_2Cl_2 and toluene, but are insoluble in hexane. The IR spectra of the (por)$Ru(ArNO)_2$ complexes (as KBr pellets) show new bands in the 1346–1350 cm^{-1} range assigned to the ν_{NO} of the coordinated ArNO groups. Employing the ^{15}N-labeled ligand results in a shift of the band at 1348 cm^{-1} (overlapping with a porphyrin band) in the IR spectrum of the unlabeled analog (TTP)Ru($N(O)C_6H_4OMe$-*p*)$_2$ to 1318 cm^{-1}, consistent with the assignment of this band as ν_{NO} ($\Delta\nu_{NO}$ −30 cm^{-1}; expected shift of −24 cm^{-1} based on a simple two-body model). In our previous work with nitrosobenzene ruthenium porphyrins,[13] we were not able to observe the formation of the putative (por)Ru(CO)(PhNO) intermediates by IR spectroscopy, suggestive of the fast conversion of (por)Ru(CO) to (por)$Ru(PhNO)_2$. We were also not able to observe, by IR spectroscopy, any intermediates during the reaction of *o*-tolNO with (por)Ru(CO) to generate (por)Ru(*o*-tolNO)$_2$. We determined that the reaction of (TTP)Ru(CO) with 4-nitrosoanisole required high temperatures to generate the (TTP)$Ru(ArNO)_2$ product. Indeed, when the reaction was performed in CH_2Cl_2 at room temperature, the intermediate complex (TTP)Ru(CO)-($N(O)C_6H_4OMe$-*p*) was observed by IR spectroscopy (ν_{CO} 1967 cm^{-1}), indicative of the slow substitution of CO by the second 4-nitrosoanisole. The ν_{CO} of this intermediate is 31 cm^{-1} higher in energy than that of the starting (TTP)Ru(CO) at 1936 cm^{-1} in CH_2Cl_2. This feature of an increased ν_{CO} suggests that the 4-nitrosoanisole ligand acts as a π-acid ligand toward the (TTP)Ru(CO) fragment, resulting in decreased backbonding of electron density into the π* orbitals of CO, thus raising ν_{CO}. We previously observed a similar IR spectral result from the reaction of (OEP)Ru(CO) with *N*,*N*-dimethyl-4-nitrosoaniline.[11] Indeed, the less efficient substitution of CO in (por)Ru(CO) by 4-nitrosoanisole, and by *N*,*N*-dimethyl-4-nitrosoaniline, is likely due to the contribution of the dipolar resonance form shown in Fig. 1.

The ^1H NMR spectra of the bis-nitrosoarene complexes in $CDCl_3$ show peaks for the coordinated ArNO ligands in addition to the peaks typical of the porphyrin macrocycles associated with the diamagnetic Ru^{II} center. The ^1H NMR spectra of the *p*-substituted tetraphenylporphyrin complexes, namely the (TTP)$Ru(ArNO)_2$ compounds, show only one set of *o*-H peaks and one set of *m*-H peaks for the *meso*-aryl substituents on the porphyrin rings, suggestive of axial symmetry in these complexes or fast rotation of the porphyrin aryl substituents on the NMR time scale. The pyrrole-H resonances of the porphyrin macrocycles occur in the narrow 8.52–8.57 ppm range.

Mono-nitrosoarene complexes

We were interested in preparing ruthenium nitrosoarene complexes of the form (por)Ru(ArNO)(L) (L = pyridine or imidazole derivative) as models of *C*-nitroso adducts of histidine–liganded heme. Reactions of the (por)$Ru(ArNO)_2$ complexes with pyridine or 1-MeIm produce the mono-nitrosoarene derivatives as shown in Scheme 2. The (por)Ru(ArNO)(py) (por = TPP, TTP) and (por)Ru(ArNO)(1-MeIm) compounds (por = TPP, TTP; ArNO = *o*-tolNO, $N(O)C_6H_4OMe$-*p*, $N(O)C_6H_2Me_2OMe$-*p*) are readily prepared *via* these substitution reactions. The pyridine complexes were obtained in 67–71% isolated yields, and the 1-methylimidazole complexes were obtained in 58–78% isolated yields. These red–purple mono-nitrosoarene complexes are moderately air-stable, showing no signs of decomposition in air after 1 month in the solid state

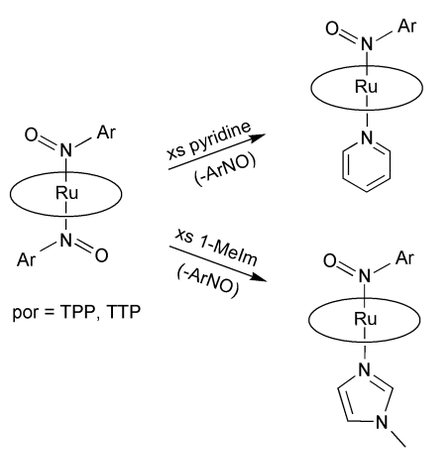

Scheme 2

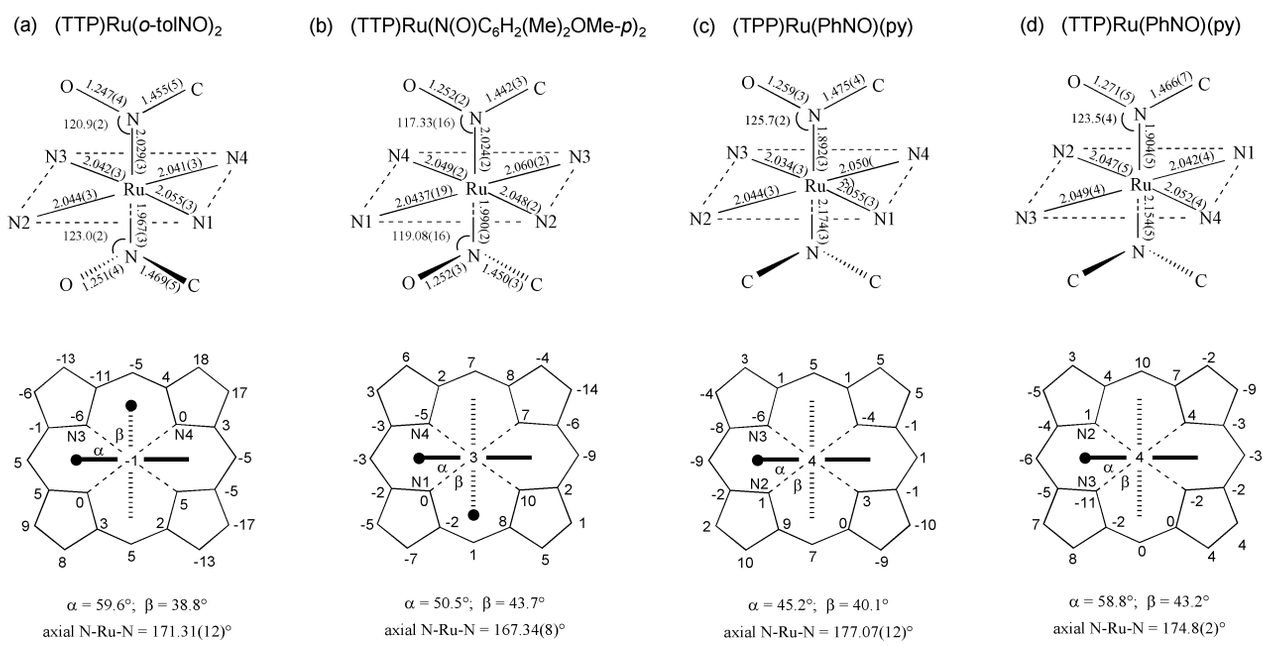

Fig. 5 Structural data for the (por)Ru(ArNO)$_2$ and (por)Ru(PhNO)(py) complexes. Selected bond lengths and angles are shown at the top. Perpendicular atom displacements from the 24-atom porphyrin plane (in 0.01 Å units) are shown at the bottom. Also shown are the axial ligand orientations: α is the torsion angle involving O–N–Ru–N(por), and β is the torsion angle involving O–N–Ru–N(por) (for (por)Ru(ArNO)$_2$) or C–N–Ru–N(por) (for (por)Ru(PhNO)(py)). The solid dot represents the nitroso oxygen atom, and the solid line represents the O–N–C unit of the ArNO ligand situated above the porphyrin plane. The dashed line represents the O–N–C unit of the second ArNO ligand situated below the porphyrin plane (for (por)Ru(ArNO)$_2$), or the C–N–C unit of the pyridine ligand (for (por)Ru(PhNO)(py)) situated below the porphyrin plane.

and at least 8 h in solution. They are readily soluble in CH_2Cl_2 and toluene, but are insoluble in hexane.

The ^{1}H NMR spectra of the crude product mixtures in $CDCl_3$ (after 30 min reaction in CH_2Cl_2 at room temperature) revealed the quantitative conversion of (por)Ru(ArNO)$_2$ to (por)Ru(ArNO)L (L = py or 1-MeIm), together with the presence of the unreacted excess pyridine or 1-MeIm. This suggests that only one ArNO ligand in the (por)Ru(ArNO)$_2$ complexes is susceptible to substitution by pyridine or 1-MeIm under our reaction conditions. Furthermore, unlike the case of the bis-nitrosoarene complex preparations, where we observed a temperature dependence of the CO substitution depending on the type of ArNO ligand used, the substitution reactions of (por)-Ru(ArNO)$_2$ by pyridine or 1-MeIm proceed at room temperature for all the nitrosoarene ligands employed in this study.

The IR spectra of the (por)Ru(PhNO)(py) complexes (as KBr pellets) show bands in the 1328–1332 cm^{-1} range assigned to ν_{NO}. These bands are 20 cm^{-1} (for TPP) and 14 cm^{-1} (for TTP) lower than those of their (por)Ru(PhNO)$_2$ precursors,[13] and the lower wavenumbers are consistent with the replacement of one PhNO ligand in (por)Ru(PhNO)$_2$ with the more basic pyridine ligand and subsequent increased Ru⟶PhNO backdonation of electron density.

The IR spectra of the (por)Ru(ArNO)(1-MeIm) complexes (as KBr pellets) also show one or two new band(s) in the 1306–1323 cm^{-1} range assigned to ν_{NO}. These ν_{NO} bands are slightly lower than those of the (por)Ru(PhNO)(py) analogues, reflecting the better electron-donating ability of the 1-MeIm ligand to the (por)Ru moiety relative to the pyridine ligand. The ^{1}H NMR spectroscopic results are also consistent with this view (see later). Interestingly, two ν_{NO} bands of comparable intensity are observed in the IR spectra of bulk samples of three of the (por)Ru(ArNO)(1-MeIm) complexes (as KBr pellets), namely (TPP)Ru(*o*-tolNO)(1-MeIm), (TTP)Ru(N(O)C$_6$H$_4$OMe-*p*)-(1-MeIm) and (TTP)Ru(N(O)C$_6$H$_2$Me$_2$OMe-*p*)(1-MeIm). For example, the IR spectrum of (TTP)Ru(N(O)C$_6$H$_4$OMe-*p*)-(1-MeIm) shows two strong bands at 1323 and 1306 cm^{-1}. Both these bands are assigned as ν_{NO} by the comparative analysis of the IR spectrum of the ^{15}N-labeled nitroso analogue (*i.e.*, ν_{NO} 1323 and 1306 cm^{-1}, $\nu_{^{15}NO}$ = 1296 and 1275 cm^{-1}, $\Delta\nu_{NO}$ −27 and −31 cm^{-1}; expected shifts of −24 and −23 cm^{-1}, respectively, based on a simple two-body model). A likely explanation is that the presence of the π-interacting and unsymmetrical 1-MeIm ligand results in two axial ligand conformations in these complexes.

As expected, the ^{1}H NMR spectra of the mono-nitrosoarene complexes (in $CDCl_3$) also reveal the peaks due to both the coordinated ArNO and pyridine or 1-MeIm ligands. The chemical shifts of the pyrrole protons of the nitrosoarene complexes prepared in this study decrease slightly in the order (por)-Ru(ArNO)$_2$ (8.52–8.57 ppm) > (por)Ru(ArNO)(py) (8.42 ppm) > (por)Ru(ArNO)(1-MeIm) (8.37–8.38 ppm), indicative of a slightly increased electron density on the porphyrin macrocycles in the mono-nitrosoarene complexes relative to the bis-nitrosoarene complexes, and in the imidazole complexes relative to the pyridine complexes.[23] This ^{1}H NMR feature is also consistent with the IR spectroscopic results discussed earlier. Furthermore, the similar chemical shift values observed for the pyrrole protons in each class of compounds indicate the similar π-accepting abilities of the ArNO ligands used in this work. The ^{1}H NMR spectra of the *p*-substituted tetraphenyl complexes (TTP)Ru(ArNO)(py) and (TTP)Ru(ArNO)(1-MeIm) reveal the inequivalence of the *o*-H protons and the *m*-H protons of the *meso*-aryl substituents on the porphyrin rings.

X-Ray crystallographic characterization

We were able to crystallize and obtain X-ray crystal structures for two members of each of the (por)Ru(ArNO)$_2$, (por)-Ru(PhNO)(py) and (por)Ru(ArNO)(1-MeIm) classes of compounds, and one example from each class is shown in Figs. 2–4. Selected metrical data for the complexes are summarized in Figs. 5 and 6. Perpendicular atom displacements of the atoms in the porphyrin skeleton from the 24-atom mean porphyrin plane and the axial ligand orientations are also shown in Figs. 5 and 6.

As can be seen in Figs. 2 and 5, the nitrosoarene ligands in the bis-nitrosoarene complexes are bound to the Ru^{II} centers *via* the η^1-N bonding mode, similar to that observed for the four other (por)Ru(ArNO)$_2$ compounds that have been structurally

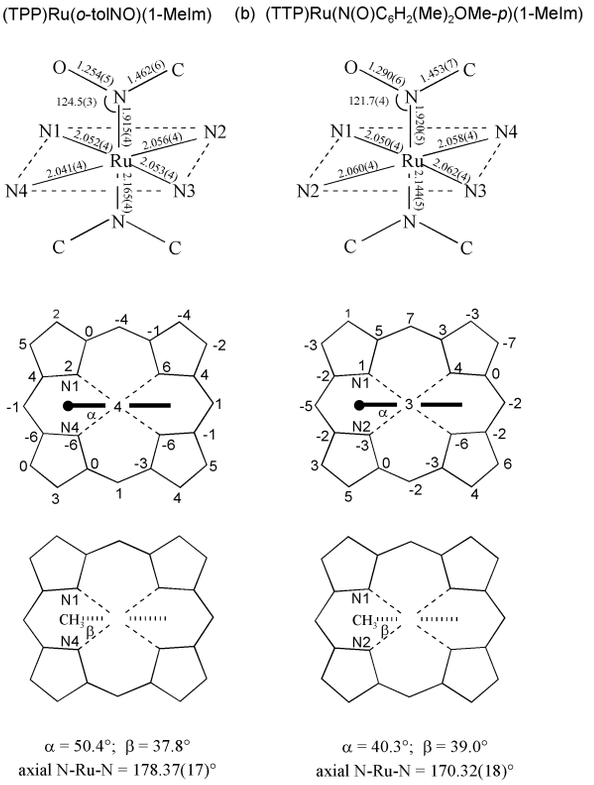

Fig. 6 Structural data for the (por)Ru(ArNO)(1-MeIm) complexes. Selected bond lengths and angles are shown at the top. Perpendicular atom displacements from the 24-atom porphyrin plane (in 0.01 Å units) are shown at the middle. Also shown are the axial ligand orientations at the middle and the bottom: α is the torsion angle involving O–N–Ru–N(por), and β is the torsion angle involving C–N–Ru–N(por). The solid dot represents the nitroso oxygen atom, and the solid line represents the O–N–C unit of the ArNO ligand situated above the porphyrin plane. The dashed line represents the C–N–C unit of the 1-MeIm ligand situated below the porphyrin plane.

characterized to date.[11–13] The ArNO ligands in (por)-Ru(ArNO)$_2$ are oriented perpendicular to each other, and their C–NO groups essentially bisect porphyrin nitrogens (Fig. 5(a) and (b)). Similar axial ligand orientations have been observed in other bis-nitrosoarene complexes of Fe,[4] Ru,[11–13] and Os,[24] and have been attributed to favorable overlap between the filled HOMO orbitals of the M^{II} centers (namely the d_{xz} and d_{yz} orbitals) with the π* orbitals of the ArNO ligands.

The nitrosobenzene ligands of the two (por)Ru(PhNO)(py) (por = TPP, TTP) compounds are also bound to the Ru^{II} center in an η^1-N fashion (Figs. 3 and 5). The axial Ru–N(PhNO) bond lengths fall in the 1.892(3)–1.904(5) Å range, and are *shorter* than those of (TPP)Ru(PhNO)$_2$ (1.953(2) and 2.049(2) Å;[13] 1.954(3) and 2.052(3) Å [12]). Such a shortening is consistent with an *increased* electron donation to the Ru center by the pyridine ligands relative to the displaced PhNO ligands and increased Ru⟶PhNO backdonation of electron density, as suggested by the IR and ^{1}H NMR spectroscopic results presented and discussed earlier. The axial ligand orientations observed for (por)Ru(PhNO)(py) are very similar to those observed for (por)Ru(ArNO)$_2$. Thus, the PhNO and pyridine ligands in (por)Ru(PhNO)(py) are oriented perpendicular to each other (Fig. 5(c) and (d)), an observation that suggests moderate π-acid character for the pyridine ligand when located trans to the π-acid ArNO ligand.

The X-ray crystal structures of the two mono-nitrosoarene compounds containing the axial 1-MeIm ligands (*e.g.*, Fig. 4) present an interesting comparison with the other structures described in this work. The axial Ru–N(ArNO) bond lengths in the two (por)Ru(ArNO)(1-MeIm) complexes fall in the 1.915(4)–1.920(5) Å range, and are similar to those determined for the pyridine derivatives (*i.e.*, shorter than the related bond lengths in the bis-nitrosoarene complexes) and reflect the basic character of the 1-MeIm and pyridine ligands and the predominant π-acid character of the ArNO ligands. Unlike the (por)Ru(ArNO)$_2$ and (por)Ru(PhNO)(py) complexes, the ArNO and 1-MeIm ligands in crystals of the ordered (por)-Ru(ArNO)(1-MeIm) complexes are oriented essentially parallel to each other, and their C–N–O (for ArNO) and C–N–C (for 1-MeIm) groups essentially bisect porphyrin nitrogens (Fig. 6). This suggests a moderate π-donor character of the 1-MeIm ligand in these mono-nitrosoarene complexes. Although the IR spectral results reveal two ν_{NO} bands suggestive of two orientations of the 1-MeIm ligands in the bulk samples, the observation of only one 1-MeIm orientation in the crystal structures may simply be due to crystal preparation or selection. Thus, it is possible that other (por)Ru(ArNO)(1-MeIm) complexes may possess non-parallel axial ligand orientations. Indeed, a preliminary X-ray crystallographic analysis of (TTP)Ru(*o*-tolNO)-(1-MeIm) (data not included) reveals a *non*-parallel arrangement of the axial disordered ArNO and 1-MeIm ligands. Furthermore, we have very recently observed a nearly-perpendicular arrangement of nitosoalkane and 1-MeIm ligands in (TPP)Fe(*i*-PrNO)(1-MeIm).[7] This is consistent with the observation of nearly perpendicular arrangements of the *C*-nitroso ligands and the *trans*-axial histidine imidazole planes in the protein complexes legHb(PhNO)[2] and Mb(EtNO).[3]

The largest deviations from the strict linearity for the axial N–Ru–N bonds are observed for the very bulky (2,6-dimethyl-4-nitrosoanisole)-containing complexes (*i.e.*, (TTP)-Ru(N(O)C$_6$H$_2$Me$_2$OMe-*p*)$_2$ (167.34(8)°) and (TTP)Ru(N(O)-C$_6$H$_2$Me$_2$OMe-*p*)(1-MeIm) (170.32(18)°)). This implies that the deviations from strict linearity could be (at least partly) determined by sterics, although deviations from strict linearity in group 8 metalloporphyrins may also result from intrinsic electronic factors.[25,26]

Summary

We have prepared a new series of six-coordinate ruthenium porphyrins containing nitrosoarene ligands. The symmetrical (por)Ru(ArNO)$_2$ and unsymmetrical (por)Ru(ArNO)(L) (L = py or 1-MeIm) complexes were studied by spectroscopy and by X-ray crystallography. In all the complexes studied, the ArNO ligands are bound to the ruthenium centers through the nitroso N-atoms. IR and NMR spectroscopic results suggest a predominant π-acid character of the ArNO ligands in these complexes. The ArNO ligands in (por)Ru(ArNO)$_2$ are oriented perpendicular to each other and essentially bisect porphyrin nitrogens, consistent with the ArNO ligands behaving as π-acids in these complexes. Thus, the perpendicular orientation of the two axial π-acid ligands maximizes the π-backbonding from two filled dπ orbitals (*i.e.*, d_{xz} and d_{yz} orbitals) of the low-spin (por)Ru^{II} fragment into the empty π* orbitals of the axial ArNO ligands. The axial Ru–N(ArNO) bond lengths (1.967(3)–2.029(3) Å) in the bis-nitrosoarene complexes are slightly longer than the related axial Ru–N(ArNO) distances of 1.892(3)–1.904(5) Å (for the pyridine complexes) and 1.915(4)–1.920(5) Å (for the 1-MeIm complexes) seen in the mono-nitrosoarene complexes, suggestive of *decreased* Ru–N(O)Ar backbonding in (por)Ru(ArNO)$_2$ relative to those in (por)Ru(PhNO)(py) and (por)Ru(ArNO)(1-MeIm). Although the IR and ^{1}H NMR spectral results suggest that the 1-MeIm ligands in the mono-nitrosoarene complexes show a slightly stronger overall electron-donating ability than the pyridine ligands, there are no significant differences in the axial Ru–N(ArNO) distances within the mono-nitrosoarene complexes containing pyridine or 1-MeIm ligands in the solid state. The O–N(Ar) bond lengths are also not significantly different within these bis- and mono-nitrosoarene complexes.

Differences in the axial ligand orientations in the (por)-Ru(ArNO)$_2$ and (por)Ru(PhNO)(py) *vs.* the (por)Ru(ArNO)-

(1-MeIm) suggest a prominent role of the metal dπ orbitals in the binding of the nitrosoarene ligands. Menyhárd and Keserú [27] reported recently that proximal histidine orientations in myoglobin play a role in NO ligand dissociation from myoglobin. We are currently in the process of designing experiments to investigate the role that the axial ligand orientations play in the dissociation and reaction chemistry of the nitrosoarene ligands.

Acknowledgements

We thank the National Science Foundation of the USA for funding for this work (Grant No. CHE-0076640). The Bruker (Siemens) SMART APEX diffraction facility was established at the University of Idaho with the assistance of the NSF-EPSCoR program and the M. J. Murdock Charitable Trust, Vancouver, WA, USA.

References

1 J. Lee, L. Chen, A. H. West and G. B. Richter-Addo, *Chem. Rev.*, 2002, **102**, 1019–1065.
2 I. P. Kuranova, A. V. Teplyakov, G. V. Obmolova, A. A. Voronova, A. N. Popov, D. M. Kheiker and E. G. Arutyunyan, *Bioorg. Khim. (in Russian)*, 1982, **8**, 1625–1636 (PDB codes 1LH4 and 2LH4).
3 D. M. Copeland, A. H. West and G. B. Richter-Addo, *Proteins: Struct. Funct. Genet.*, 2003, **53**, 182–192.
4 L.-S. Wang, L. Chen, M. A. Khan and G. B. Richter-Addo, *Chem. Commun.*, 1996, 323–324.
5 N. Godbout, L. K. Sanders, R. Salzmann, R. H. Havlin, M. Wojdelski and E. Oldfield, *J. Am. Chem. Soc.*, 1999, **121**, 3829–3844.
6 D. Mansuy, P. Battioni, J.-C. Chottard, C. Riche and A. Chiaroni, *J. Am. Chem. Soc.*, 1983, **105**, 455–463.
7 C. D. Sohl, J. Lee and G. B. Richter-Addo, Presented at the 225th National Meeting of the American Chemical Society; March 23–27, 2003, New Orleans, LA, USA, 2003. Abstract INORG 166; manuscript in preparation.
8 R. F. Loeb, A. V. Bock and R. Fitz, *Am. J. Med. Sci.*, 1921, **161**, 539–546 (*Chem. Abstr.*, 1921, 51:1761).
9 W. Filehne, *Arch. Exptl. Pathol. Pharmakol.*, 1878, **9**, 329.
10 C. Crotti, C. Sishta, A. Pacheco and B. R. James, *Inorg. Chim. Acta*, 1988, **141**, 13–15.
11 L. Chen, J. B. Fox, Jr., G.-B. Yi, M. A. Khan and G. B. Richter-Addo, *J. Porphyrins Phthalocyanines*, 2001, **5**, 702–707.
12 J.-L. Liang, J.-S. Huang, Z.-Y. Zhou, K.-K. Cheung and C.-M. Che, *Chem. Eur. J.*, 2001, **7**, 2306–2317.
13 J. Lee, B. Twamley and G. B. Richter-Addo, *Can. J. Chem.*, 2002, **80**, 1252–1258.
14 S. J. Fox, L. Chen, M. A. Khan and G. B. Richter-Addo, *Inorg. Chem.*, 1997, **36**, 6465–6467.
15 Taken in part from: J. Lee, PhD Thesis, University of Oklahoma, 2002.
16 D. P. Rillema, J. K. Nagle, L. F. Barringer, Jr. and T. J. Meyer, *J. Am. Chem. Soc.*, 1981, **103**, 56–62.
17 E. Bosch and J. K. Kochi, *J. Org. Chem.*, 1994, **59**, 5573–5586.
18 N. G. Connelly, P. T. Draggett, M. Green and T. A. Kuc, *J. Chem. Soc., Dalton Trans.*, 1977, 70–73.
19 SMART: v.5.059: Bruker Molecular Analysis Research Tool, Madison, WI, 1997–1998.
20 SAINTPlus: Data Reduction and Correction Program. Version 6.02, Madison, WI, 1998.
21 G. M. Sheldrick, SADABS (Siemens Area Detector ABSorption Correction Program), Madison, 1999.
22 G. M. Sheldrick, SHELXTL : Structure Determination Software Suite, Madison, WI, 1998.
23 J. W. Buchler, W. Kokisch and P. D. Smith, *Struct. Bonding (Berlin)*, 1978, **34**, 79–134.
24 L. Chen, M. A. Khan, G. B. Richter-Addo, V. G. Young, Jr. and D. R. Powell, *Inorg. Chem.*, 1998, **37**, 4689–4696.
25 G. B. Richter-Addo, R. A. Wheeler, C. A. Hixon, L. Chen, M. A. Khan, M. K. Ellison, C. E. Schulz and W. R. Scheidt, *J. Am. Chem. Soc.*, 2001, **123**, 6314–6326.
26 G. R. A. Wyllie and W. R. Scheidt, *Chem. Rev.*, 2002, **102**, 1067–1089.
27 D. K. Menyhárd and G. M. Keserú, *J. Am. Chem. Soc.*, 1998, **120**, 7991–7992.